

Don't throw rocks from the side-lines: The Effect of “Wave Breakers” on the Magnetohydrodynamic Instability in Aluminum Reduction Cells

Pedcenko, A, Molokov, S & Bardet, B

Author post-print (accepted) deposited by Coventry University's Repository

Original citation & hyperlink:

Pedcenko, A, Molokov, S & Bardet, B 2016, 'The Effect of “Wave Breakers” on the Magnetohydrodynamic Instability in Aluminum Reduction Cells ' *Metallurgical and Materials Transactions B*, vol 48, no. 1, pp. 6-10

<http://dx.doi.org/10.1007/s11663-016-0840-5>

DOI 10.1007/s11663-016-0840-5

ISSN 1073-5615

ESSN 1543-1916

The final publication is available at Springer via <http://dx.doi.org/10.1007/s11663-016-0840-5>

Copyright © and Moral Rights are retained by the author(s) and/ or other copyright owners. A copy can be downloaded for personal non-commercial research or study, without prior permission or charge. This item cannot be reproduced or quoted extensively from without first obtaining permission in writing from the copyright holder(s). The content must not be changed in any way or sold commercially in any format or medium without the formal permission of the copyright holders.

This document is the author's post-print version, incorporating any revisions agreed during the peer-review process. Some differences between the published version and this version may remain and you are advised to consult the published version if you wish to cite from it.

- 1
- 2
- 3

4

5

6

8

9

10

11
12
13
14
15
16
17

1 Introduction

The effective control of magnetohydrodynamic (MHD) instabilities in aluminium reduction cells is the problem of great importance. The process of primary aluminium production (aluminium smelting) is based on the electrolytic reduction of the metallic aluminium from its high melting point oxide: alumina (2345 K (2072°C)). In this technology, known as Hall-Héroult process, the alumina is dissolved in molten cryolite ¹, which lowers its melting point and improves its electric conductivity. This solution is contained at 1233 K (960°C) in large (e.g. 13×4×0.3m) rectangular cells – electrolytic pots, with graphite top and bottom lining, serving as the anode and cathode electrodes respectively. High electric current of several hundreds kA is then passed through the cell, and, as a result of the electrochemical reaction, the liquid aluminium "pad" is formed under the cryolite, at the bottom of the cell. The process is relatively expensive due to the amount of electricity required for the reduction of each kilogramme of aluminium (11...14 kWh). The main loss of energy is due to low electric conductivity of cryolite, so reducing its thickness by every millimetre can result in substantial savings worldwide.

Unfortunately, when the cryolite thickness² is reduced below a certain threshold, such a binary system of two immiscible fluids with the vast difference in their electrical conductivities and very small difference in densities, becomes unstable owing to the electromagnetic body force. This force appears due to the interaction of the horizontal component of the electric current and vertical component of the background magnetic field, produced by the bus bars supplying electricity to the cell. This interfacial instability, being magnetohydrodynamic in nature, is known to produce sloshing or "rolling-pad" waves [4] at the interface between the cryolite and aluminium, propagating along the perimeter of the cell in a rotating fashion. Such disturbances of the interface can reduce effectiveness of the smelting process and disrupt the normal operation of the cell or even the whole pot-line. Thus, the control and suppression of unstable surface waves is one of the important problems in aluminium smelting.

Since pioneering work by T. Sele [4], who identified the basic mechanism for the interface motion, many theoretical studies were devoted to the under-

¹sodium aluminium fluoride salt

²known also as the anode to cathode distance, ACD

standing of the impact of different technological factors on the fluid motion in the aluminium layer. Experimental investigation of the phenomenon, however, is quite complicated due to the lack of safe and accessible experimental modelling materials with the required physical properties. One of the possible solutions proposed in [1] is to replace in the model the poorly conducting cryolite with an array of 30×30 , $\varnothing 2\text{mm}$ -thin, vertical stainless steel electrodes, which when immersed in the liquid metal, supply the electric current to its free surface and do not obstruct its vertical motion. Because the effective electric resistance of such an array of thin conductors is about 100 times higher than that of liquid metal, the tilt of the interface will result in the redistribution of the electric current between all parallel electrodes. This creates a horizontal component of the current j_{\perp} in the better conducting liquid metal, as the current needs to spread there before entering less conductive bottom of the cell. Externally imposed vertical magnetic field \vec{B} of a sufficient strength (up to 100 mT) triggers a horizontal motion of the liquid metal due to the appearance of the electromagnetic Lorentz force $\vec{j} \wedge \vec{B}$, eventually resulting in the rolling surface wave with a growing amplitude. Such a physical model does not pretend to replicate the entirety of electrodynamic processes occurring in the real cell, but it mimics the basic principle of the Sele-type MHD instability and thus is dynamically similar to the instability in real cells. The advantages of this experimental model have been discussed in [1]. The present report is an extension of the previous experimental study published in [1] and modelling work presented in [2].

2 Presentation of the problem

One of the possible ways to suppress the sloshing motion of a fluid is to introduce obstacles (i.e. "wave breakers"). For example, partitioning walls or baffles are used in tankers to suppress a surge or sloshing of liquids during transportation.

Song *et al.* in [5] report some slowing down of the liquid metal using "cathode with protrusions" in both numerical and industrial trials of . Dupuis and Bojarevics ([6],[7],[8]) report that the overall damping effect is not that significant, but all agree that such protrusions can increase the horizontal current in the liquid metal, which is responsible for the instability onset. It seems that the balance between these two effects will determine the success or otherwise of such a cathode construction. In our study we use non-conductive

”protrusions”, which have no influence on the current distribution in the liquid metal, and their role is purely hydrodynamic.

The experimental cell (Fig.2) used in this work has the same construction as in [1]: 30×30 cm square box filled with 2-5 cm thick layer of room-temperature liquid metal alloy In-Ga-Sn. To prevent the oxidation of liquid metal and overheating of thin anode electrodes, the gap between the free surface of the liquid metal and the top anode plate was filled with weak 3% HCl water solution. As the obstacles (further referred to as WB), the identical plexiglass bars of the 10×15 mm cross-section, placed across the width of the cell and attached to its bottom, were used. In different tests, their number (from 1 to 7) and the arrangement were changed. Fig. 1a shows schematic view of the experimental cell with only one WB in the middle, while Fig. 1b shows 3D view of the cell with 5 WB uniformly spread along its bottom. The external uniform vertical magnetic field (10...80 mT) generated by two induction coils was applied throughout the cell.

The height of WB was kept the same 1.5 cm in all the trials, and was chosen to be less than the minimum height of the liquid metal layer (2 cm) in order not to partition the cell into separate compartments, but to allow the motion of liquid metal across the whole cell.

3 Methodology

The measurements of free surface oscillations in the unstable regime of the cell were taken for different WB configurations and melt heights. Recordings were performed using video camera (Fig.2), which was filming the middle area of the front wall of the cell at 30 fps. This allowed to detect the instantaneous height of the liquid metal at that particular location during the passage of the wave. Later, the video data was post-processed, and the time-history of the surface oscillations extracted with the accuracy of about ± 0.1 mm.

Before introducing any obstacles in the melt, the test case without them was recorded for every height of the liquid metal layer ($h_0 = 20, 35, 50$ mm) at different values of the anode current I and vertical magnetic field B . This case served as a reference data for later tests with different WB arrangements (Fig.3). Normally, in a single test run for one height of the melt, different WB configurations were tested. To keep the melt level constant, the small amount of In-Ga-Sn alloy was taken out or added into the cell in order to compensate for the volume occupied by WB.

122 The general procedure was the following: the desired WB arrangement
 123 was installed in the cell and the required height of the melt was set. The top
 124 anode plate with 900 stainless steel electrodes (see Fig.2) was lowered for the
 125 tips of the electrodes to immerse into the liquid metal for $1 \pm 0.25\text{mm}$ below
 126 the free surface. Then relatively high values of the anode current I and the
 127 magnetic field B were set to trigger the onset of the wave.

128 After that, both I and B were lowered to the desired values. Then the
 129 magnetic field was kept constant and the current I was lowered in small
 130 steps. At each step of the current magnitude, a video recording of the sur-
 131 face oscillations was taken. Then the procedure was repeated for a different
 132 magnetic field value B , and so on. For each B , a certain minimum value of
 133 the anode current I_{min} was found, at which the cell became stable. This pair
 134 of B_{min} and I_{min} values was recorded as the '*lower thresholds*'. The set of
 135 such B_{min} and I_{min} combinations was found for each WB arrangement and
 136 represented the stability curve, below which the cell is stable.

137 4 Results and discussion

138 Fig.3 shows the reference case of lower threshold values B and I for when
 139 no WB were installed in the cell. The magnetic field was varied between 5
 140 and 80 mT, and the anode current was varied between 100 and 1200 A. The
 141 uncertainty of each experimental point on this graph, i.e of finding the lowest
 142 I_{min} value while keeping B constant, is several amperes.

143 One can see that the curves follow some sort of inverse function $\sim I^{-1}$ and
 144 the higher melt level h_0 generally leads to a more stable cell. The amplitude
 145 of the wave is proportional to the product of B and I .

146 Fig.4 shows the standard deviation of the free surface oscillations, ob-
 147 tained from the video recordings, as a function of the anode current I and
 148 the magnetic field B for one height of the melt (35 mm). The amplitude
 149 of oscillations grows linearly with respect to the anode current, however its
 150 sensitivity to the change in magnetic field B is different: at low B values the
 151 growth is close to linear, but then saturates at higher magnetic field.

152 Now we take the first melt level, $h_0 = 20\text{mm}$, fix magnetic field at about
 153 the midrange $B = 50\text{mT}$, and introduce several WB configurations. Fig.5
 154 shows the obtained surface oscillations with none, one and three WB, ar-
 155 ranged in parallel to each other at equal spacings along the width of the cell
 156 (as in Fig.1). As seen from the graph, the addition of even one WB lowers the

157 RMS of oscillations by $\sim 35\%$ compared to the control case. Three obstacles
 158 reduce the RMS by another $\sim 25\%$. The last curve in Fig.5 has been obtained
 159 with "cross-breaker", which consisted of two single WBs, perpendicular to
 160 each other and crossing at the centre of the cell. One can see that such a
 161 WB arrangement is damping oscillations most effectively for $h_0 = 20\text{mm}$, i.e.
 162 when the relative height of the obstacle is $0.75h_0$. Indeed, because the super-
 163 position of two sloshing modes along each horizontal direction comprises the
 164 overall "rolling" wave, such WB configuration is affecting the sloshing in each
 165 of these directions. Finally, Fig.6 shows the lower thresholds of the instability
 166 for melt level $h_0 = 20\text{ mm}$. This confirms the gradual improvement of the
 167 melt stability from none to one and three WB cases. The "cross-breaker"
 168 case, which showed lowest amplitude of the surface oscillations, from the
 169 stability point of view, lies somewhat in between 1 and 3 WB arrangements.

170 Stability results for $h_0 = 35\text{ mm}$ are shown in Fig.7. Now the relative
 171 WB height is $0.43h_0$ and it is clear that the performance of WB starts to
 172 deteriorate: everything below 3 WB has basically no effect on the stability
 173 thresholds. Further increase of the number of WB's makes no improvements
 174 over 3WB case (we also tested 5WB and 7WB parallel arrangements).

175 Increasing the melt height even further to $h_0 = 50\text{ mm}$, results in almost
 176 no influence of WB's on the stability thresholds. The relative WB height
 177 now is only $0.3h_0$. Fig.8 shows the results of previously most effective 3WB
 178 case for this melt level.

179 The frequency of the free surface oscillations was also found to decrease
 180 with the introduction of obstacles in the liquid metal. The frequency spectra
 181 of the wave was recovered from the video recordings for two heights of the
 182 liquid metal $h_0 = 20$ and 35 mm . The base frequency for the control case
 183 without WB agrees well with the natural frequency of the wave f_0 , which
 184 can be easily calculated from the expression for the propagation speed c
 185 of the internal gravity waves at the interface between two liquids in a shallow
 186 binary layer: $c = \sqrt{\Delta\rho g / (\rho_0/h_0 + \rho_1/h_1)}$, where ρ_0 and ρ_1 are densities of
 187 the liquid metal and top fluid (water) respectively, $\Delta\rho$ is their difference,
 188 g is the acceleration due to gravity and $h_1 = 5\text{cm}$ is the height of the top
 189 fluid. The base frequency f_0 , Hz, of the wave is then obtained as $f_0 = c/\lambda$,
 190 where $\lambda = 0.6\text{ m}$ is the wave length (half of the cell perimeter). Thus, the
 191 calculated base frequencies are $f_0 = 0.66\text{ Hz}$ for $h_0 = 20\text{ mm}$ and $f_0 =$
 192 0.85 Hz for $h_0 = 35\text{ mm}$. They are in a very good agreement with the ones
 193 observed experimentally; see Table 1, which shows experimental values of f_0

194 for different WB configurations.

195 5 Conclusions

196 The experimental tests investigating the influence of the different configura-
197 tions of "wave-breakers" on the rolling-pad surface instability were performed
198 in the low-temperature laboratory model. The effectiveness of these configura-
199 tions was assessed by analysing the data of the stability thresholds and the
200 RMS values of the free surface oscillations. At the high relative height of the
201 obstacles ($0.75h_0$) the pronounced suppression of the waves was observed:
202 up to 50% (for 3WB) by RMS value. In this case the frequency of the wave
203 (hence its celerity) was also found to decrease by $\sim 15\%$ for 3WB and cross-
204 WB cases. For the higher melt level $h_0 = 35$ mm, when the relative height
205 of the obstacles becomes $0.43h_0$, the suppression effect was found to be less
206 pronounced, leaving only 3WB configuration as the only one effective: sur-
207 face oscillations decreased by $\sim 30\%$ (RMS) and the wave propagation speed
208 by 8%. Finally, at $h_0 = 50$ mm (WB height is $0.3h_0$) the damping effect of
209 the obstacles was practically unnoticeable.

210 The outcomes of this study had an important industrial impact: the
211 results were used by Rio-Tinto for the development and validation of the full
212 3D numerical model of electrolysis cell, which allowed them to increase the
213 productivity of its plants while lowering the environmental footprint. This
214 and the subsequent numerical works [9, 10] led to a patent [11].

215 References

- 216 [1] A. PEDCHENKO, S. MOLOKOV, J. PRIEDE, A. LUKYANOV AND
217 P. J. THOMAS: *EPL*, 2009, vol. 88(2), p.24001
- 218 [2] S. RENAUDIER, B. BARDET, G. STEINER, A. PEDCENKO, J. RAPPAZ,
219 S. MOLOKOV AND A. MASSEREY: *TMS Light Metals*, 2013, pp.577–584
- 220 [3] J. F. GERBEAU, C. L. BRIS AND T. LELIÈVRE: *Mathematical Methods*
221 *for the Magnetohydrodynamics of Liquid Metals*, Oxford University Press,
222 New York, 2006, pp.233–286.
- 223 [4] T. SELE. *Metallurgy Transactions B*, 1977, vol.8(4), pp.613–618

- 224 [5] Y. SONG, P. JIANPING, D. YUEZHONG, W. YAOWU, L. BAOKUAN
225 AND F. NAIXIANG: *Metall. Res. Technol.*, 2016, vol.113(3), p.7
- 226 [6] M. DUPUIS, V. BOJAREVICS: *TMS Light Metals*, 2014, pp.479–482
- 227 [7] M. DUPUIS, V. BOJAREVICS: *TMS Light Metals*, 2015, pp.821–826
- 228 [8] M. DUPUIS, M. PAGÉ: *TMS Light Metals*, 2016, pp.909–914
- 229 [9] G. STEINER. Simulation numérique de phénomènes MHD: Application
230 l'électrolyse de l'aluminium Thesis number 4469, EPFL, 2009.
- 231 [10] S. FLOTRON. Simulations numériques de phénomènes MHD-thermiques
232 avec interface libre dans l'électrolyse de l'aluminium Thesis number 5738,
233 EPFL, 2013.
- 234 [11] S. RENAUDIER AND B. BARDET. Electrolysis tank with slotted floor.
235 patent WO2015017925, 2013.

Configuration	f_0 , Hz ($h_0 = 20$ mm)	f_0 , Hz ($h_0 = 35$ mm)
No WB	0.67	0.86
1 WB	0.65	0.84
3 WB	0.58	0.79
1 cross-WB	0.57	0.77

Table 1: Base frequency f_0 of the wave measured for different WB configurations at two heights h_0 of the liquid metal layer.

236 Figure Captions

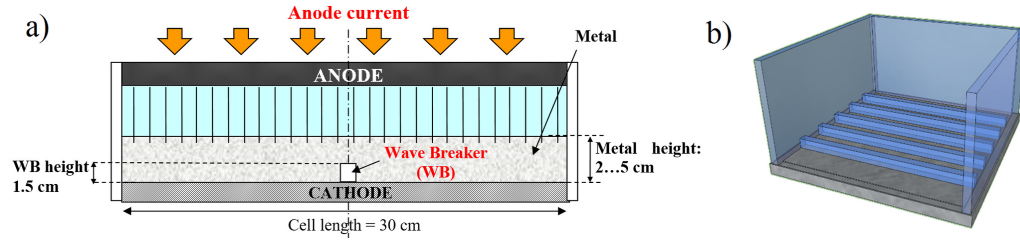


Figure 1: (a) Side view of the experiment with 1 WB installed in the middle of the cell; (b) 3D view of the cell (one side wall removed) with 5 WB equally spaced along its width.

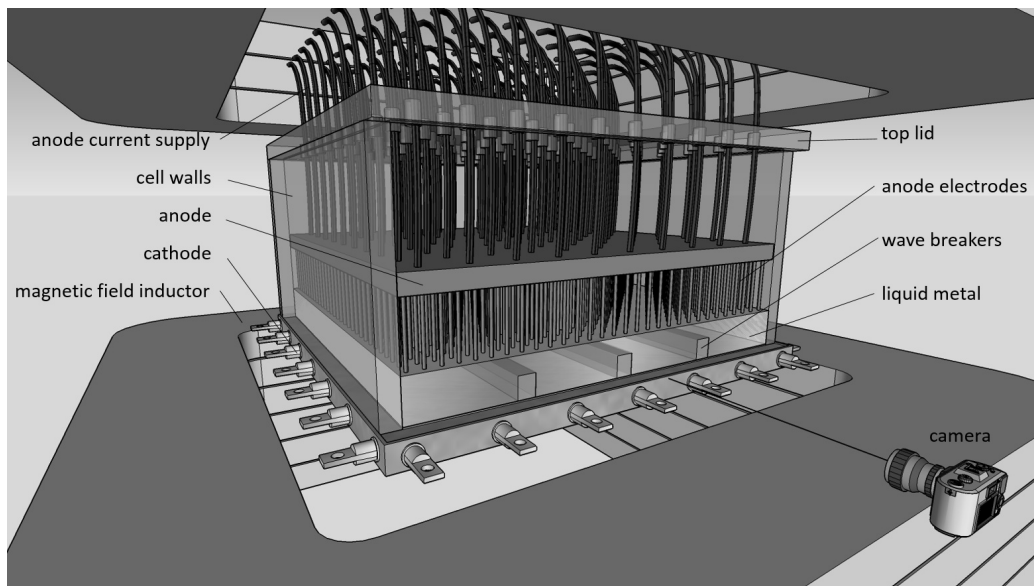


Figure 2: 3D view of the test cell inside the inductor coils.

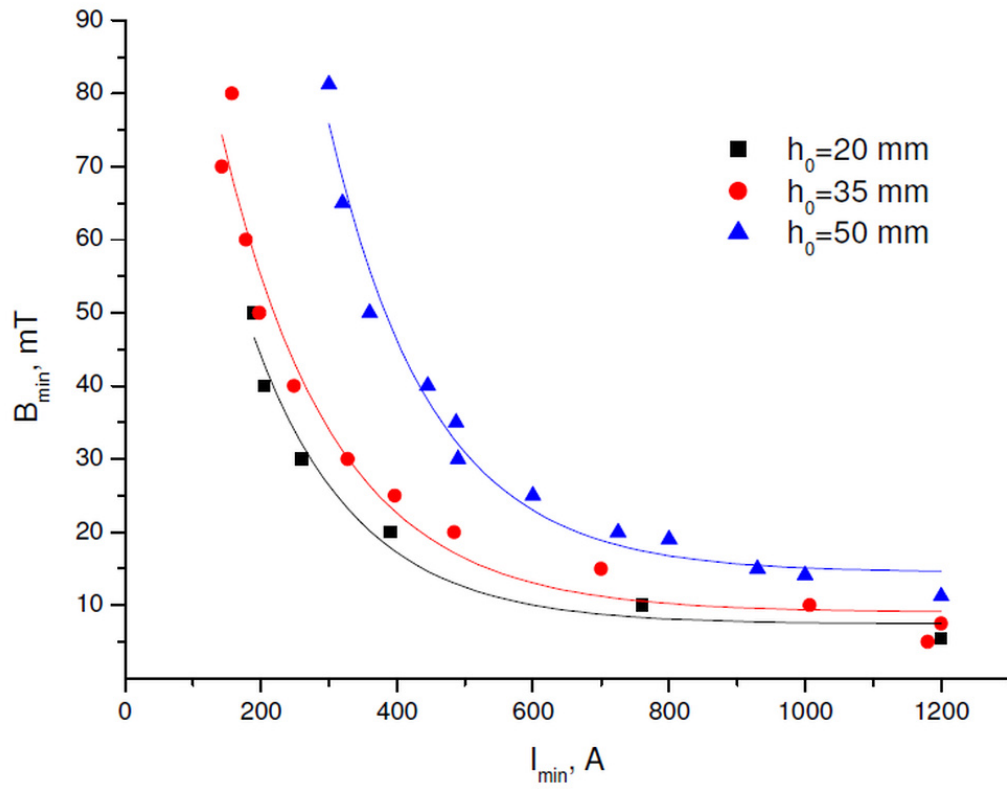


Figure 3: Lower threshold curves of $B(I)$ for three melt levels $h_0 = 20, 35, 50$ mm without 'wave breakers'.

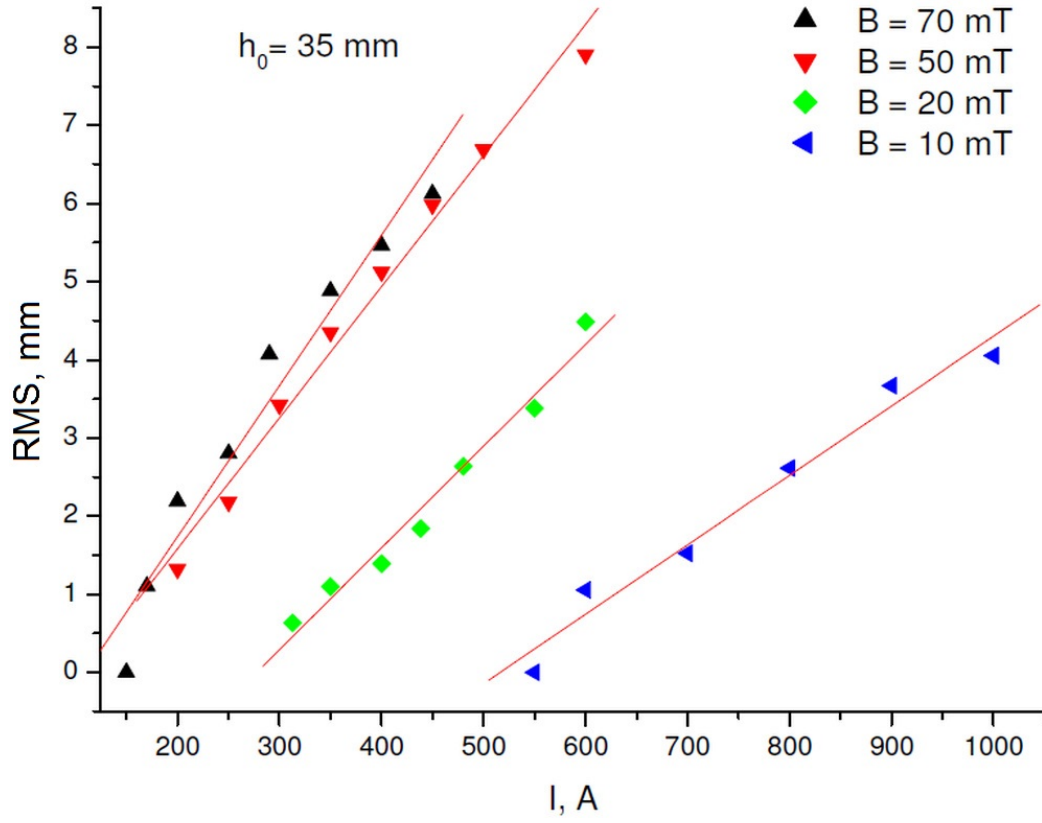


Figure 4: RMS value of the surface oscillations vs. anode current I , A for different values of magnetic field B and single melt height $h_0 = 35$ mm without 'wave breakers'.

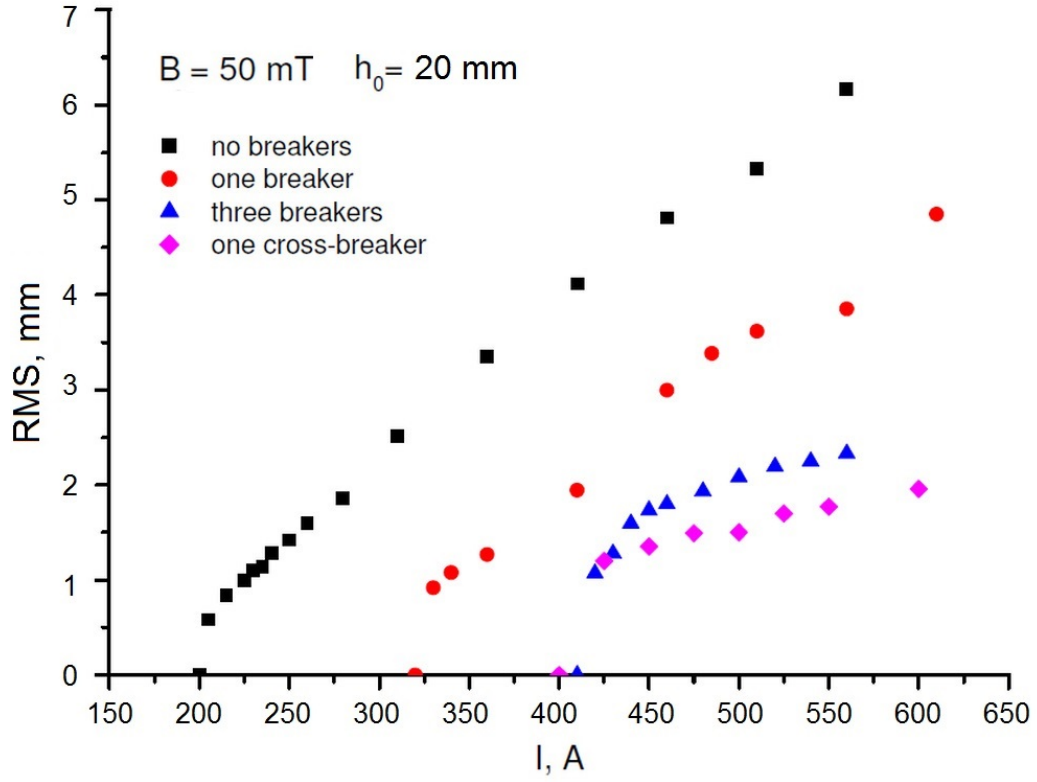


Figure 5: RMS value of the surface oscillations vs. anode current I , A for magnetic field $B = 50$ mT and melt height $h_0 = 20$ mm with different WB arrangement.

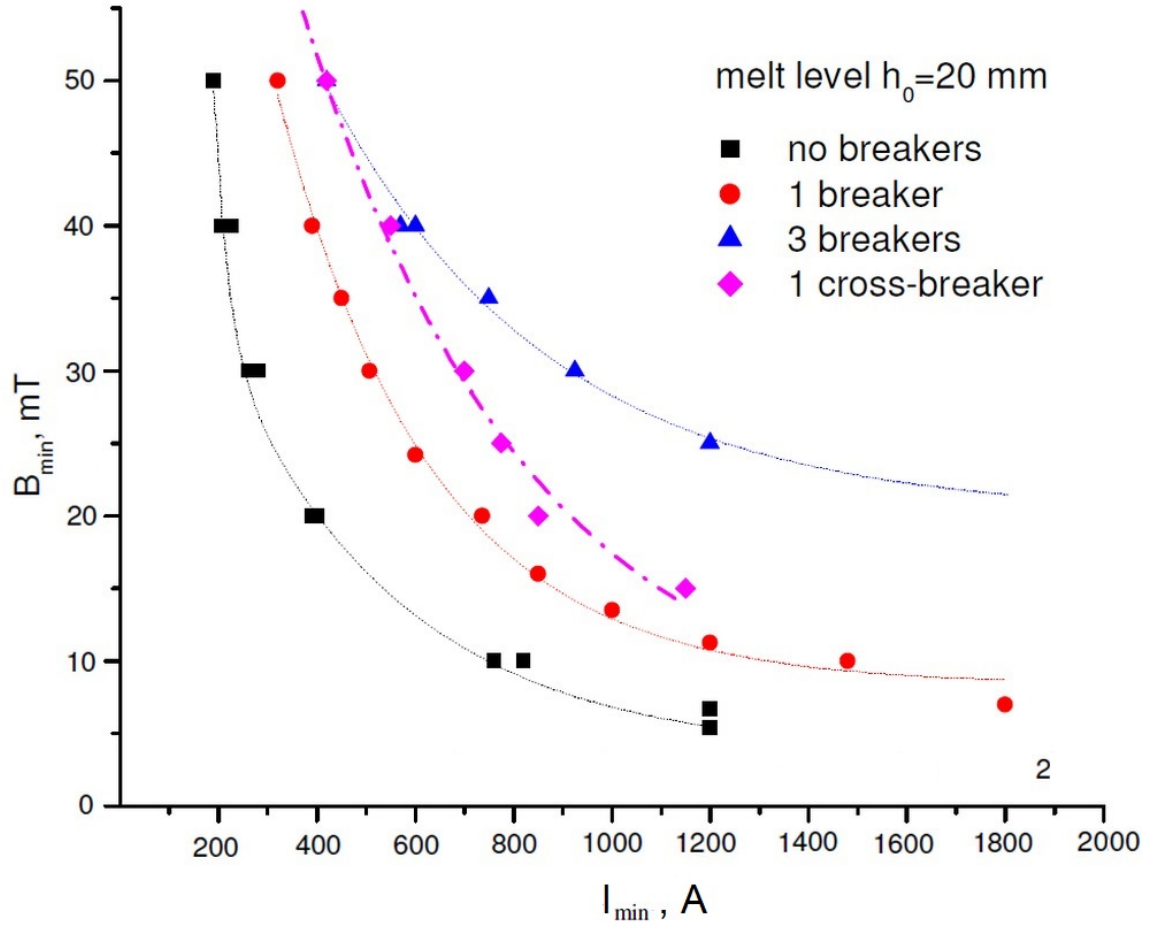


Figure 6: Stability thresholds for melt level $h_0 = 20$ mm and different WB arrangements.

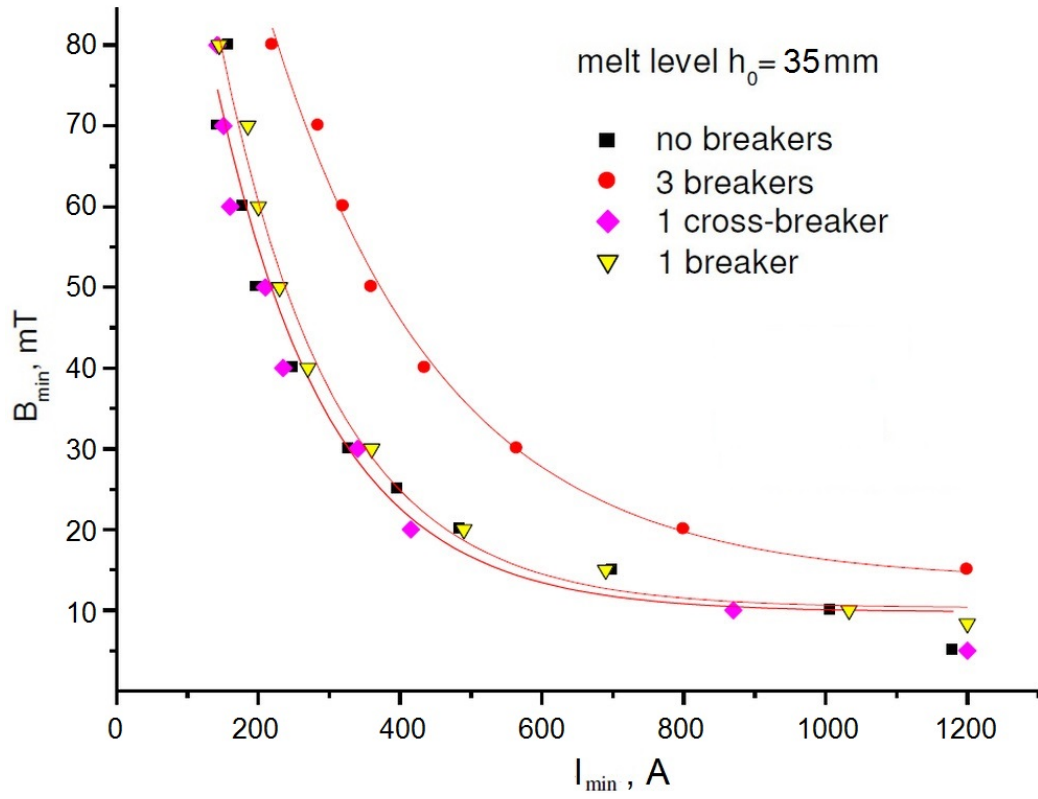


Figure 7: Stability thresholds for melt level $h_0 = 35\text{ mm}$ and different WB arrangements.

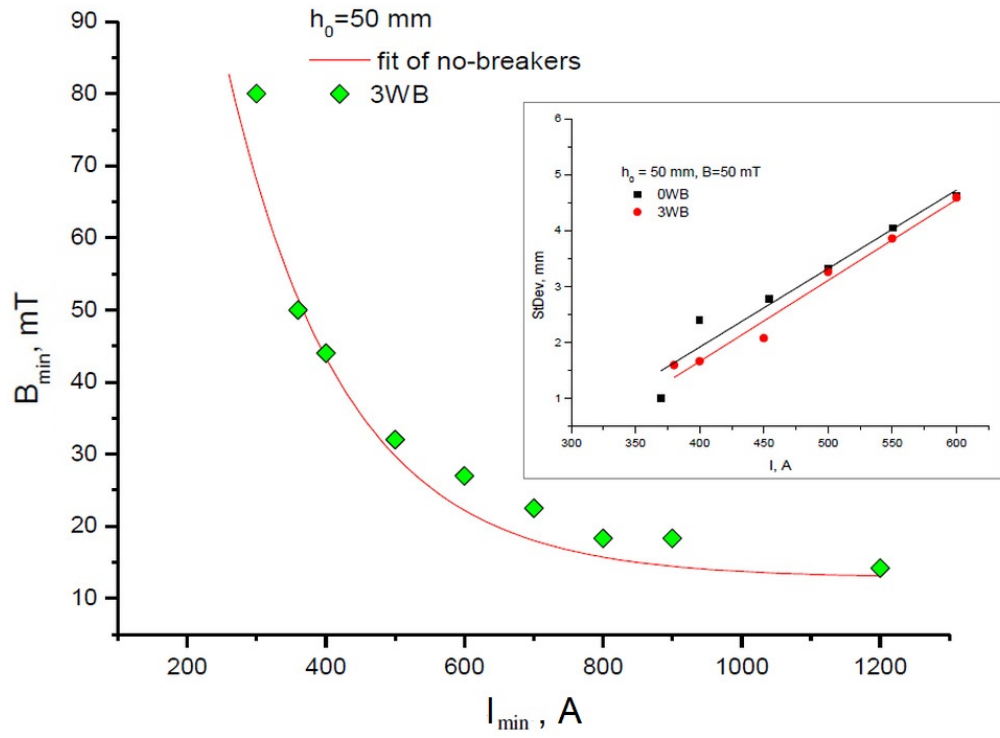


Figure 8: Stability thresholds for $h_0 = 50$ mm: no WB (solid line) and 3WB. Insert shows the 3WB influence on the RMS value of surface oscillations vs. no-WB case for $h_0 = 50$ mm.